Journal of Geochemical Exploration 183 (2017) 88–101

Contents lists available at ScienceDirect

Journal of Geochemical Exploration

journal homepage: www.elsevier.com/locate/gexplo

Discovery of the Hendou-abad copper mineral district and its association to dikes: A reconstruction scenario for exploration of Cu-porphyry, northeast Isfahan, Iran

Zahra Alaminia[a,*], Maryam Salehi[a], Fritz Finger[b]

[a] Department of Geology, Faculty of Sciences, University of Isfahan, Azadi square, P.O. Box 81746-73441, Isfahan, Iran
[b] Department of Chemistry and Physics of Materials, University of Salzburg, Jakob Haringer Straße 2a, A-5020 Salzburg, Austria

ARTICLE INFO

Keywords:
Mafic dike swarm
Breccia
Hydrothermal alteration
Hendou-abad Cu mineral district

ABSTRACT

The Hendou-abad copper mineral district is located along the eastern margin of the central part of Urumieh–Dokhtar Magmatic Arc (UDMA). The mineralization is hosted in the Late Eocene basaltic andesite and trachybasalt, where it is associated with epidote, calcite, and quartz as alteration minerals, and red, white, and green breccias. Two main events of mineralization with alteration have been distinguished: hypogene and supergene. Abundant parallel dike swarms intrude Late Eocene volcanic rocks of the Henduo-abad. The Hendou-abad dikes are seen as a few cm to 4 m wide and < 1200 m long. The purpose of this work was to survey their petrogenesis and the tectonic implication of the dikes. Further, to investigate the relationship between dikes and known copper mineralization in Hendou-abad, and then examine exploration potential in adjacent areas. The Hendou-abad dikes, based on trend, relative age, and geochemical composition, are divided into two groups: early and late dikes. The geochemical character of these dikes displays an arc setting and the late dikes show higher contents of Nb, Zr, P, K, Rb, Ba, and slightly elevated Ti. The geochemical composition of the dikes suggests two magmatic stages over time: a subduction-modified mantle source is thought of for the host basaltic andesites and the early dikes in a primitive arc stage, while an enriched asthenospheric mantle source is pictured for the late dikes in a later, more mature arc stage. Structural evidences from field-work of dikes, strike-slip and thrust faults, and microscopic studies of the associated hypogene mineralization imply that they may have formed through north-south directed extension during an uplift event. The pattern of dike orientations, their intense propylitic alteration, and the spatially association with mineralized breccias, sheeted calcite, and mineralized quartz veins, could suggest emplacement of a porphyry stock at depth. Our data show that the east-trending green dikes are associated with red and green breccias in southern Ardestan and that they could be used as an exploration target for copper mineralization.

1. Introduction

The Urumieh–Dokhtar Magmatic Arc (UDMA) is endowed with significant porphyry and epithermal ore deposits, such as Sungun, Kahang, and Sarcheshmeh in northwest, central, and southeast UDMA, respectively (Aghazadeh and Badrzadeh, 2015; Alavi et al., 2014; Afzal et al., 2012; Shahabpour, 2005). Sungun, Sarcheshmeh and a number of subeconomic porphyry copper deposits are dominated by Middle Miocene stocks (Shahabpour, 1982; Bertrand et al., 2014; Richards and Sholeh, 2016). The Ardestan mining region (Fig. 1B) along the eastern side of central UDMA is also well known for a number of economically significant Cu deposits of varying sizes and ore grades (e.g., Dorojin and Zafarghand, Fig. 1C) that are dominantly hosted in the Eocene-Oligocene volcanic rocks. It is well established that copper deposits can be associated with plutonic rocks in arc setting (Kerrich and Wyman, 1997; Tosdal and Richards, 2001; Richards, 2005; Sillitoe, 2010). Numerous studies of southeast Ardestan rocks have focused on the intermediate to felsic intrusive rocks (Sadeghian and Ghaffary, 2011; Sarjoughian and Kananian, 2017). Kananian et al. (2014a) focused on the Nasrand pluton and its dikes and proposed fusion of continental crust in their petrogenesis. Jabbari et al. (2010) suggest a temperature of 700° to 1114 °C and a pressure of 2.4 to 7.7 kbar for the igneous crystallization of the dikes, using clinopyroxene thermobarometry on the similar dikes of southwest Ardestan. Sarjoughian (2017) recently studied the Nasrand dikes and reported a temperature of 940 °C, emplacement depth of 11.4 km, and magmatic water contents of 4.6 wt%

* Corresponding author.
E-mail address: z.alaminia@sci.ui.ac.ir (Z. Alaminia).

http://dx.doi.org/10.1016/j.gexplo.2017.10.006
Received 7 May 2017; Received in revised form 13 September 2017; Accepted 4 October 2017
Available online 05 October 2017
0375-6742/

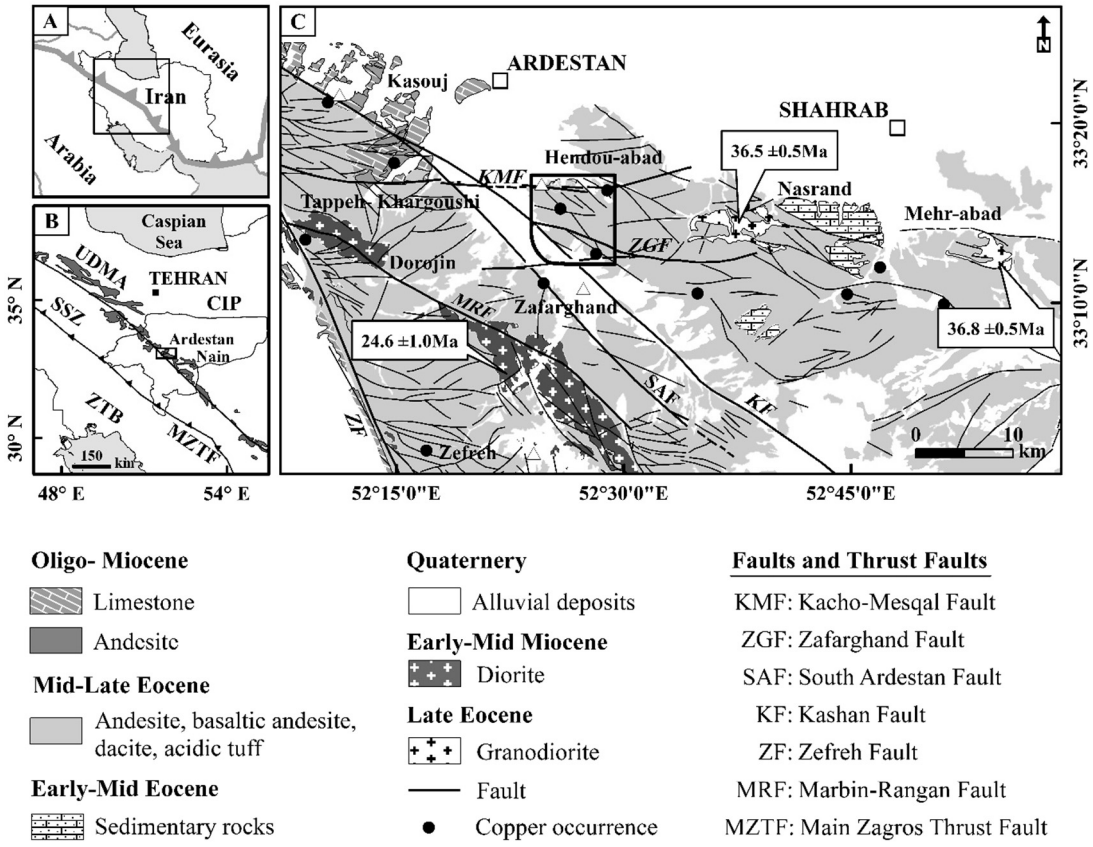

Fig. 1. (A) Location of Neotethyan suture in Iran. (B) Position of Ardestan copper-bearing range in Isfahan province and central part of UDMA. (C) Simplified geologic map of the Ardestan copper-bearing range. Modified after Radfar and Amini Chehragh (1999) and Bahroudi and Fonoudi (2000). Mehr-abad, Zafarghand and Nasrand granodiorite ages are from Sarjoughian and Kananian (2017). Hendou-abad mineral district is situated approximately 12 km southeast of Ardestan between KMF and ZGF.

in the dikes. The volcanic rocks in east Ardestan- west Nain were classified into five groups by Yeganehfar et al. (2013): including older Late Oligocene (26.5 Ma) high-Nb mafic rocks and younger Early Miocene (18.7 Ma) adakitic volcanic rocks as endmembers of age and composition. Their age estimates are consistent with zircon U-Pb age dating of Chiu et al. (2013), who reported 30.1 and 26.3 Ma for two samples of ignimbrite and andesite in northwest Nain.

In general, few studies describe the mechanism of formation of the mafic dike swarms in this area of Iran. This study presents new field observations and characteristics of major- and trace-element composition of dikes from the Hendou-abad copper mineral district. The dynamic structural environment of dikes is discussed. The development of these mafic dikes is thought to be related to the mineralization spatially, temporally, and structurally. The goal of this research is to interpret the evolution of tectonic events and examine dikes in the area in order to determine their relationship relative to the events of copper mineralization.

2. Geologic setting

2.1. Tectonic evolution

Tectonically, the regional geology of Isfahan includes four different provinces (Fig. 1B), the central Iranian Plate (CIP) in the east, UDMA, and Sanandaj-Sirjan Zone (SSZ) in the center, and the Zagros Thrust Belt (ZTB) in the west. The west boundary of the SSZ is defined by the Main Zagros Thrust Fault (MZTF), a northwest-trending suture zone. All terranes above, excluding the first one, belong to the youngest preserved orogenic event in the world, namely, the Zagros uplift (Fig. 1B). The Zagros orogeny was formed as a consequence of the protracted convergence of Eurasia and Arabia (inset map in Fig. 1) and the closure of the Neo-Tethys Ocean (e.g., Berberian and King, 1981; Sengor, 1990; Verdel et al., 2011) and their subsequent collision. The northeasterly direction of subduction of Neo-Tethys below the central Iranian plate resulted in the 10^6 km^2 (Verdel et al., 2011) of basaltic to rhyolitic volcanic rocks and gabbroic to granitic plutonic rocks in the UDMA during the Eocene-Oligocene (e.g., Ghasemi and Talbot, 2006; Dargahi et al., 2010; Chiu et al., 2013) and even younger between the Middle Miocene to Pliocene (e.g., Axen et al., 2001; Azizi and Moinevaziri, 2009). Although unlike an island arc (e.g., Alavi, 1996; Ghorbani, 2006; Shahabpour, 2007; Yeganehfar et al., 2013), some researchers have proposed an active continental margin geodynamic framework for the UDMA (e.g., Berberian and Berberian, 1981; Moinvaziri, 1985; Verdel et al., 2011; Ayati et al., 2012). More recently, Yeganehfar et al. (2013) in a detailed geochemical study of the volcanic rocks (extending from west Nain to Ardestan) concluded that they represented a transient, rather enriched asthenospheric mantle for Late Oligocene rocks. According to some of the previous studies, several immature back-arc basins formed during initiation of subduction in the CIP during Upper Triassic-Lower Jurassic, such as Nain-Baft (Ghazi and Hassanipak, 1999; Agard et al., 2005), Sabzevar (Alaminia et al., 2013), and Sistan in Middle Jurassic-Upper Cretaceous (Fotoohirad et al., 2009). Closure of these oceans occurred during the Cretaceous-Paleocene (Rosseti et al., 2010). However, the recent findings show an extensional environment for inner arc and back arc of the Urumieh–Dokhtar (Ghasemi and Rezaei, 2015). The former studies propose that the Eocene-Paleocene (60–40 Ma) extrusive event in UDMA occurred in a shallow marine setting (Berberian and King, 1981) probably related to crustal attenuation (thinning) (Berberian and Berberian, 1981; Morley et al., 2009; Agard et al., 2011) and appears to represent both arc and back-arc volcanism (e.g., Vincent et al., 2005) with a calc-alkaline affinity (e.g., Shahabpour, 2007). The Qom Formation marks an isolated branch

of the Tethyan Seaway that was located north of the main ocean (Harzhauser and Piller, 2007). Verdel et al. (2011) suggested Late Paleocene-Eocene magmatic flare up was extension related. The numerous intrusions of calc-alkaline and alkaline composition (Moinvaziri, 1985), are composed of various rocks including gabbro, diorite, granodiorite, and granite bodies of Late Eocene to Post Miocene or Pliocene (Mohajjel et al., 2003; Chiu et al., 2013; Sarjoughian and Kananian, 2017) in the UDMA. These were interpreted as pre- to *syn*-collisional (Arvin et al., 2003; Shahabpour, 2005) or syn- to post-collisional intrusions (Dargahi et al., 2010).

2.2. General geology of the Ardestan area

The Ardestan copper-bearing range in Ardestan (northeastern Isfahan) is located at the eastern margin of the UDMA (Fig. 1B). The geology of Ardestan consists mostly of Eocene igneous rocks, although there are also small scattered outcrops of sedimentary rocks (Fig. 1C). The oldest rocks are sandstone and conglomerate, with intercalated limestone on the eastern side of Nasrand (Fig. 1C), which are Lower to Middle Eocene in age, based on their fossil record. The igneous rocks of Ardestan have previously been described (Radfar and Amini Chehragh, 1999; Bahroudi and Fonoudi, 2000).

According to relative age, two main sequences of volcanic rocks occur in Ardestan (Fig. 1C). The former is comprised of Middle-Late Eocene thick-bedded lava flows with more than one km thickness of compact, massive basaltic andesite and andesite (Radfar and Amini Chehragh, 1999; Bahroudi and Fonoudi, 2000). They locally grade upwards into dacite, rhyolite tuff, and volcaniclastic sediments with a Late Eocene age. The bimodal volcanic succession is cut by a diabase dike swarm of different widths (Radfar and Amini Chehragh, 1999). Most of the known copper mining districts in the region of Isfahan are associated with Late Eocene basaltic andesite to Oligocene andesite (Fig. 1C, Bahroudi and Fonoudi, 2000). Although, recent U-Pb and K-Ar radiometric dating of volcanic rocks of Ardestan indicates ages ranging from 20 to 30 Ma (Yeganehfar et al., 2013; Chiu et al., 2013). The upper part of this sequence is comprised of a thin-bedded red, acidic pyroclastic rock and of green tuff. Moreover, small outcrops of ignimbrite and pyroclastic rocks with mostly rhyolitic tuff are exposed in the southern parts of Ardestan, up to 50 m in thickness near faults (Radfar and Amini Chehragh, 1999). Due to activity of the equivalent Pyrenean orogenic events, these volcanic rocks are overlain unconformably by Late Oligocene to Early Miocene fossiliferous shallow limestone and marl (Radfar and Amini Chehragh, 1999). Exposure of this unit has an irregular morphology to the north of Kacho-Mesqal Fault (KMF) (Fig. 1C). The latter period of volcanic activity in Ardestan is Oligocene in age with lava flows of andesite (Radfar and Amini Chehragh, 1999). This altered andesite is dark greenish in colour due to the pervasive occurrence of epidote and chlorite. The andesite is interbedded with Oligo-Miocene sedimentary rocks equivalent with those of the Qom Formation.

Magmatic activity in Ardestan as a whole started in the Late Eocene with the emplacement of the main intrusions: Nasrand and Mehr-abad granodiorite batholiths with an east-west direction parallel to the KMF and was followed by Late Oligocene to Early Miocene Zafarghand and Feshark intrusions in the southern portion of the study area (Fig. 1C, Sarjoughian and Kananian, 2017). The former includes predominantly granodiorite and granite with an east-trending elongation that intruded into the volcanic rocks; low grade contact metamorphism is evident in their country rocks (Sadeghian and Ghaffary, 2011; Kananian et al., 2014b). Numerous northwest-southeast trending mafic dikes are associated with the Nasrand intrusion (Bahroudi and Fonoudi, 2000) and are used in our study (Kananian et al., 2014a).

3. Analytical methods

During field mapping of the Hendou-abad mineral district during the winter 2016, > 170 hand-sized samples of dikes and volcanic rocks as well as 17 samples from drill cores were taken from different localities, on the surface and subsurface (see Fig. 4 for sample locations). Based on petrographic observations from a set of 42 thin sections, the least-altered rocks were selected for geochemical analysis. Twelve samples of fresh dikes (early dike samples including Cu_IS20, Cu_IS44, Cu_IS101, $Cu_{II}S159$, and late dike samples including $Cu_{II}S161$, Cu_IS132, BH_5-5.2, BH_{14}-6.5, BH_5-25), least-altered trachybasalt ($Cu_{II}S75$) and epidote altered andesite ($al_{II}S41$) were analyzed by X-Ray Fluorescence (XRF) at the Salzburg University, Austria. The thorium content of dikes was reanalyzed using gamma spectrometry, because this method provides lower detection limits and better precision than XRF.

A total of 29 ore samples were investigated using transmitted and reflected microscopy, X-ray diffraction (XRD) of three samples (Cu_IS31, Cu_IS101, $Cu_{II}S159$), and lithogeochemistry (ICP-MS) of seven samples (Cu_IS26, Cu_IS52, $Cu_{II}S14$, $Cu_{II}S23$, $Cu_{II}S19$, $Cu_{II}36$ and $al_{II}S41$). Electron microprobe analysis (EMPA) of seven polished sections of ore (Cu_IS52, $Cu_{II}23$, $Cu_{II}S19$, $Cu_{II}S36$, BH_6-8) and the epidote altered andesite ($al_{II}S41$) were obtained using a Cameca SX-100 electron probe micro-analyzer at the Iranian mines and mining industries development and renovation organization (IMIDRO), Tehran, Iran. Operating conditions were an acceleration voltage of 25 kV, the beam current 20 nA, and counting time 20 s.

4. Results of field work and petrography

4.1. Field visits

4.1.1. Structural pattern

In the study area, the most prominent faults are the KF, KMF, and ZGF (Fig. 2A). The northwest-southeast trending KF structure is along the western border of the mineral district. This fault shows a dextral strike-slip component of movement, while KMF and ZGF faults (Fig. 2A) with east-west trends have reverse and dextral strike-slip components of movement along their fault planes (Beygi et al., 2016; Mohammadi, 2016). Here, structural investigation was completed using satellite images and the Ardestan geological map in 1:100000-scale (Radfar and Amini Chehragh, 1999) in combination with field visits, with an aim to characterize faults and dikes of the region. Measurements from 77 faults and 46 dikes throughout the study area were made and geometrically analyzed. Geometric analysis was carried out using Rose diagrams for faults and dikes (Fig. 2B and C). In general, the local structural pattern at the district scale identified three groups of faults and dikes consisting of the following:

1) Northwest-trending longitudinal faults (N 116 to N 167°E) with reverse and dextral strike-slip components of movements parallel to MZTF, including SAF and KF (Fig. 1C). The early dikes also extend from northwest to southeast in the study area (Fig. 2C).
2) Vertical faults at N 22 to N 45°E with sinistral movements parallel to the Zagros convergence direction.
3) East-trending faults between N 52° and N 89°E (Fig. 2A). The most important are two principal thrust faults, KMF in the north and ZGF in the south of study area. The later dikes occur mainly in this third pattern located along high-angle faults. Most of the known copper occurrences in the study area are spatially associated with east-striking faults dipping 70° to 87° to the south, and the deposits largely follow the contact with late dikes. Timing relations between these faults and mineralization are not known conclusively, but exposure of a copper vein in the east-west and northwest-southeast directions suggests that both orientations could be hosts to mineralization in the Hendou-abad mineral district.

4.1.2. Structural indicators and features

Along the margin of central Iran, there are strike-slip fault systems and thrusts (Hessami et al., 2003). The study region lies at the junction

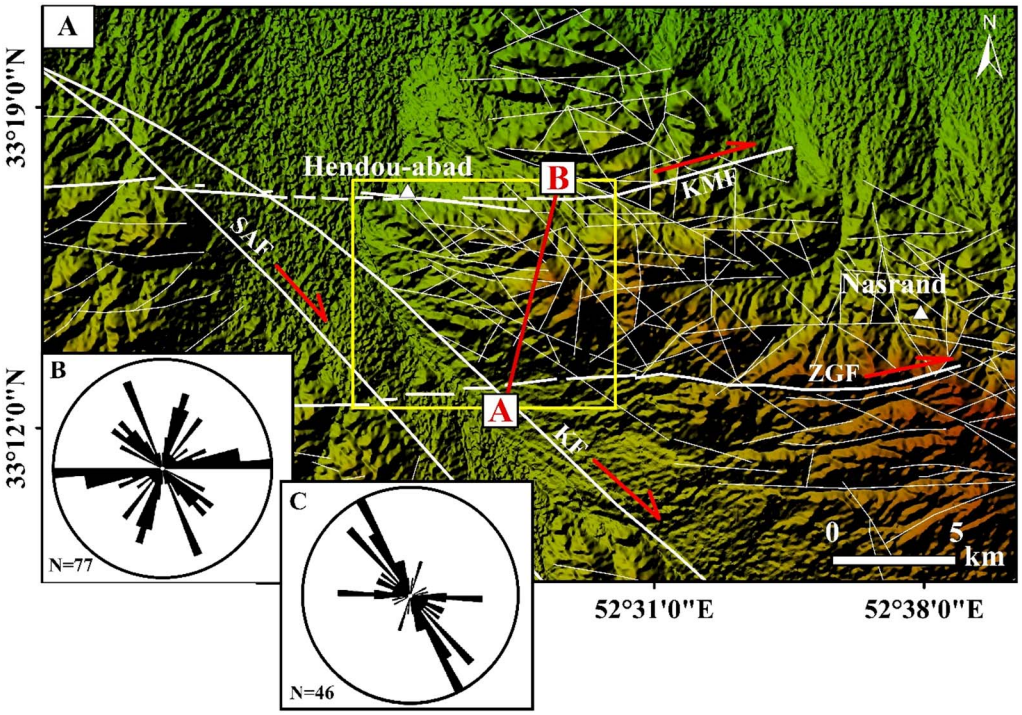

Fig. 2. (A) Digital elevation model (DEM) map illustrating the higher topography for the Hendou-abad mineral district to the north and south. The transect A–B cross-section is shown in Fig. 5. Abbreviations: KF-Kashan fault, SAF-South Ardestan fault, and KMF-Kacho-Mesqal fault. Rose diagrams showing orientation of structural data from: (B) faults compared to (C) dikes, Eeast-trend dikes are late dikes.

of two major east-west and northwest-southeast trending tectonic faults close to the extensional faulting of the eastern margin of the UDMA (Fig. 1C). Some faults are active today, with earthquakes revealing dextral motion on northwest-southeast orientated faults and sinistral motion on northeast–southwest trending faults (Walker and Jackson, 2004). Structural field investigations estimate some tilting of the recent alluvial fans near the KF and ZGF faults, and dextral motion of streams, between 10 and 180 m, near the KF fault (Fig. 3A). The oldest stage of movement observed includes vertical movements that are still creating deep valleys (Fig. 3B), vein-filled fractures (calcite sheeted veins, Fig. 3C), many high-angle normal faults south of the KMF fault (Fig. 3D), building mountains in the footwall and subsidence to the north of the KMF and south of the ZGF faults (Figs. 3B and 5). These examples from the field noted above are considered to have developed within an extensional stress regime in a north-south direction. Moreover, milky quartz veins associated with epidote alteration show sinistral displacement from 5 to 10 cm (Fig. 3F). In addition to extensional structures, the KMF and ZGF show evidence for reverse displacement (Mohammadi, 2016). It is characterized by folding in Oligo-Miocene limestone near the KMF. Some samples of epidote alteration and mineralization exhibit microstructures with undulose extension or bending seen in chalcopyrite, chalcocite, and calcite. Large quartz grains are rarely seen since they are often replaced by numerous small recrystallized grains with irregular boundaries. Epidote occurs either in lenses, bands or as space filling in tension fractures.

4.2. Geologic relationships and petrography in the Hendou-abad mineral district

Detailed field geology work associated with logging of three bore holes (total 79.6 m in length) shows the stratigraphy of the study area in Fig. 5. Rock units recognized within the Hendou-abad mineral district consist of a thick andesite to basaltic andesite sequence of Late Eocene age (Radfar and Amini Chehragh, 1999) that were intruded by mafic dikes (Fig. 4). However, K-Ar age of 26.5 ± 0.59 Ma and zircon U-Pb age of 26.3 ± 0.4 Ma have been dated by Yeganehfar et al. (2013) and Chiu et al. (2013), respectively for similar volcanic rocks in the neighboring Hendou-abad mineral district. This volcanic sequence underlies extensive areas of the mineral district and is the principal host for mineralization (Fig. 4). Additionally, local intercalations of shallow marine limestone and marl sequence and Oligocene andesite, have formed several small exposures outside of the study area to the north of the KMF fault in the vicinity of Hendou-abad village (Figs. 1C and 4). Thin bedded limestone has a thickness between 10 and 300 m. These rocks disconformably overlie the Late Eocene units (Fig. 5). An episode of deformation, during the north-south-trending shortening movements on Late Oligocene-Early Miocene limestone (Schuster and Wielandt, 1999) above, has been recognized north of the KMF that indicates several northwest-trending folds with an asymmetrical axial surface with N 100°E strike and plunge 60–70° towards northwest. Neogene conglomerate in the south study area contains rounded to subangular gravel clasts of altered volcanic, plutonic, mylonite, breccia, and silica veins. All rocks above are overlain by Quaternary alluvial deposits.

4.2.1. Late Eocene volcanic sequence

The black to dark grey volcanic rocks (Fig. 6A), classified on the basis of petrographic study of 17 thin sections, show they are mostly basaltic andesite and trachybasalt in composition, with some being andesite and relatively few are trachyandesite. Basaltic andesite is abundant and has marked red hematite colour that appears to be alteration during eruption in a sub-aerial (coastline) environment associated with *syn*-volcanic weathering. Based on field data and textural studies, eruption style of the basaltic andesite rocks is viewed as lava flows with rounded vesicles. Copper mineralization is hosted in the basaltic andesite and trachybasalt (Fig. 5).

Mineralogically, the volcanic rocks consist of medium- to fine-grained plagioclase, pyroxene, and olivine phenocrysts with a groundmass of fine-grained plagioclase and opaque minerals. Their textures are porphyritic, amygdaloidal, microlitic, intersertal, and less commonly vitrophyric. Trachyandesite and trachybasalt may show flow alignment of phenocrysts. Amygdales are filled by calcite, chlorite, zeolites, quartz, and copper oxides. In accordance with the petrographic and X-ray diffraction analyses, the volcanic rocks exhibit very low grade metamorphism of the groundmass, the open spaces, and vacuoles or even phenocrysts, indicated by the presence of secondary minerals such as epidote, chlorite, zeolite, prehnite, pumpellyite, albite,

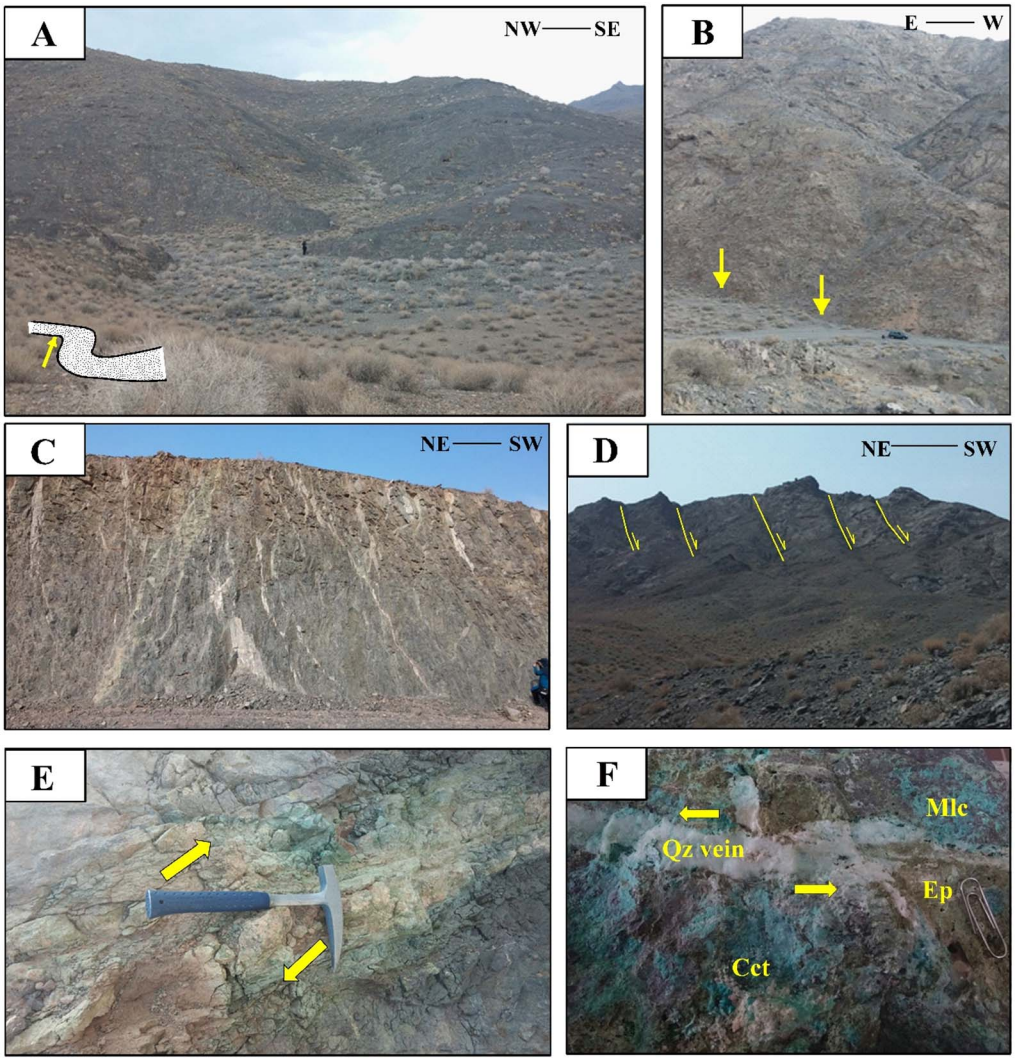

Fig. 3. Field photographs of general view representative examples of structural styles in study area, (A) dextral sense assumed from shape of stream, (B) deep valley, (C) sheeted veins of calcite, (D) parallel normal faults. Humans and car for scale. Faults in yellow, with yellow arrows pointing to inferred dip direction, (E) Right lateral movement of quartz-malachite vein by Quaternary fault (F) with left lateral displacement of west-trending epidote alteration that is associated with quartz veins. Yellow arrows show movement direction. Abbreviations used in Figs. 3, 8 and 9 (according to Whitney and Evans, 2010): Bn-bornite, Cct-chalcocite, Ccp- chalcopyrite, Cv- covellite, Dg- digenite, Dj- djurleite, Gth- goethite, Gp-gypsum, Hem-hematite, Mlc- malachite, Py- pyrite, Qz-quartz and *Si*-silica. (For interpretation of the references to colour in this figure legend, the reader is referred to the web version of this article.)

actinolite, tremolite, and calcite.

4.2.2. Dikes

The texture and mineralogy of the sampled dikes were examined. From the structural trending and the study of > 25 thin sections from a textural point of view, the dikes were divided into two groups:

1- Grey to greenish black dikes (Figs. 6B and 5) including gabbro and diorite compositions, with northwest-southeast trend (N 138° to N 160°E), dipping ~80 to 90°. They are 0.5–4 m wide and > 500 m long. These dikes are fine-grained with microlitic plagioclase (Fig. 6D), and show subophitic and aphyric textures. They contain phenocrysts of plagioclase (50–60%), clinopyroxene (< 10%),

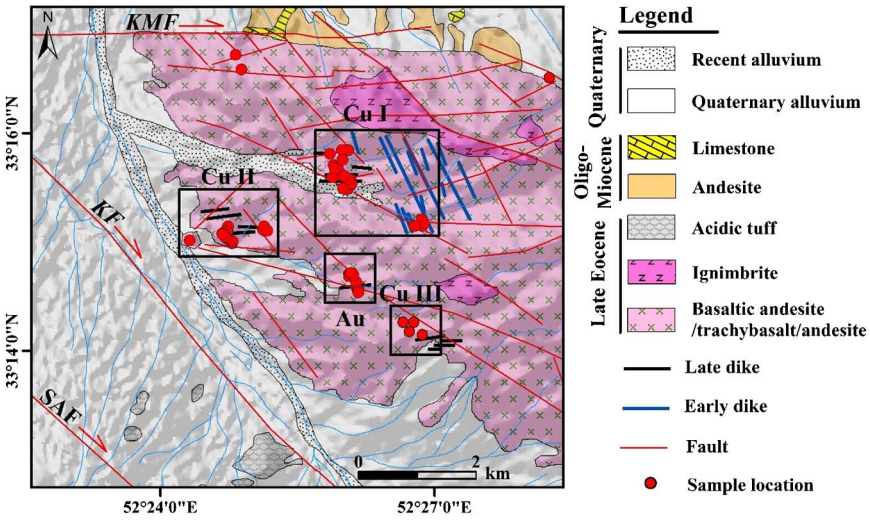

Fig. 4. Geologic map of the southeastern part of Ardestan, Hendou-abad (modified after Radfar and Amini Chehragh, 1999) including the early and late dikes, mineral district and the location of collected samples, as well as copper and gold targets.

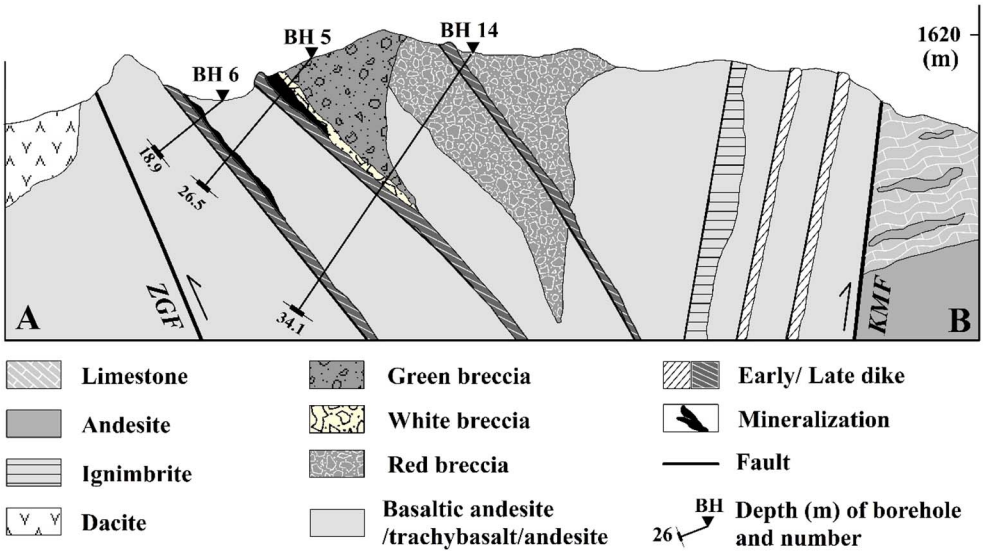

Fig. 5. Schematic geologic northeast-southwest cross section of the Hendou-abad showing field relationships along the mineral district in the area of the northeast Isfahan. BH5, BH6 and BH14 show the location of bore holes in A-B cross-section shown in Fig. 2A.

olivine (< 5%), and Fe-Ti oxides (< 5%). Accessory minerals include titanite and apatite. Secondary green to brownish-green amphibole occurs as actinolite and tremolite (10–15%). Early dikes display minerals of regional, very low grade metamorphism like the Late Eocene volcanic rocks described above.

2- Greenish dikes (Figs. 6C and 5) consist of pyroxene-bearing diorite and gabbro compositions, with east-west trend (N 90° to N 105°E), steep dip ~65 to 90°. They are 0.08–1.6 m wide, and > 100 m long. These dikes contain plagioclase (45–55%) and clinopyroxene (12–15%), with apatite, titanite, and zircon (1%), as well as opaque minerals (5–10%) of magnetite and pyrite with a porphyritic texture (Fig. 6E). Microprobe data indicate that the plagioclase and pyroxene are mostly of labradorite and augite composition, respectively. They are set in a locally altered intergranular to subophitic groundmass of plagioclase, clinopyroxene, chlorite, and calcite. This group of dikes spatially shares similar structural trend as most of the Cu-bearing veins and are parallel to the contact of the ore veins (Fig. 8B).

4.3. Breccias

Three types of breccia have been recognized in the Hendou-abad mineral district, based on time of formation, structural geometry, and cement mineralogy (altered rock flour), labeled red, white, and green breccias (Table 1).

4.3.1. Stage 1

Red breccia (Figs. 7A and 8A) is volumetrically the most abundant breccia with pipe-like morphology at the surface and a width of 3 to 10 m. It contains fragments of variable size of altered volcanic rock with rounded morphology with low proportion of matrix. The matrix consists of secondary iron oxides, carbonate, clay, and minor quartz, as well as minor primary chalcopyrite and pyrite. They are dominantly occurring with late dikes situated beside faults and crush zones. Weak

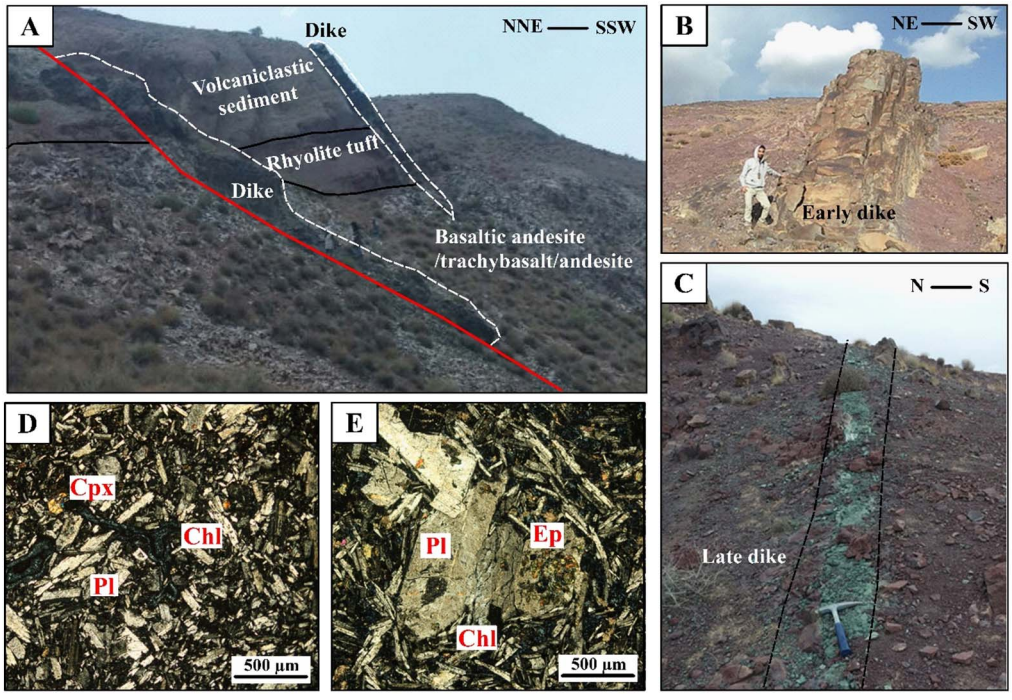

Fig. 6. Photographs and photomicrographs of: (A) Vertical section of Ardestan area showing field relationship and steep boundary between early dikes and Late Eocene volcanic rocks. Human in centre of image. (B) Early dike cutting across weathered basaltic andesite. (C) Hydrothermally altered, late dike in weathered altered basaltic andesite. (D) Photomicrograph of microlites of plagioclase in an early dike. (E) Porphyritic texture in late dike with needle-like plagioclase with chlorite in the groundmass. Plagioclase phenocryst altered to epidote.

Table 1
Summary of breccia characteristic of Hendou-abad mineral district.

Event	Geometry	Fragment form	Matrix	Infill
Red breccia	Pipe	Rounded. Up to 19 cm	Low (20 to 30%)	Calcite, clay, fine quartz, sulfide
White breccia	Vein style	Angular. Up to 2 cm	High (50 to 60%)	Quartz
Green breccia	Tabular	Angular to sub-rounded Up to 7 cm	Moderate (30 to 40%)	Epidote, calcite and fine quartz, sulfide

propylitic alteration characterizes the fragments. Carbonate and gypsum in open voids (cavities) is also observed. This milled breccia developed by a volume expansion process (Jebrak, 1997; Laznicka, 1988; Taylor, 2009) before formation of the late dikes.

4.3.2. Stage 2

White vein-like breccia zones (Figs. 7B and 8B) are 10 to 30 cm wide and are characterized by triangular, elongated wall rock fragments (locally 10–35% vol.), including red breccia and volcanic rocks, set in abundant quartz-bearing infill. The angular-shaped fragment size is highly variable (Fig. 7B). Contacts between white breccia and volcanic rocks are sharp. The white breccia commonly is oriented parallel to late dikes (Fig. 8B). Brecciation occurs at the beginning of vein formation with sharp contacts. It is likely structurally controlled.

4.3.3. Stage 3

Green hydraulic breccia (Fig. 7C and D) have a tubular geometry. Breccia infill is characterized by abundant epidote with minor calcite and fine-grained quartz. Green breccia contains 25–60% clasts that consist of rounded coarse and angular medium sized fragments of altered volcanic rocks in the margin and core of the breccia, respectively. These hydrothermal breccias are interpreted to have been emplaced during pulses of mineralization close to ore veins.

4.4. Alteration and mineralization

The following description of alteration and mineralization is based on fieldwork, core logging, and detailed studies of textural relationships. In general, alteration at the Hendou-abad mineral district was marked by the development of propylitic alteration in wall rock as pods, veins (Fig. 8C) or filled tension cracks at the regional to local scale. The alteration assemblage accompanying mineralization generally includes epidote, calcite, and quartz. Based on petrographic and X-ray diffraction analysis, other minor gangue assemblages recognized in this area consist of chlorite, clinozoisite, and actinolite with traces of titanite, pumpellyite, and prehnite. Epidote is the most abundant alteration mineral in the district. There are four kinds of epidote in the Hendou-abad mineral district, from the earliest to the latest: type I as replacement, massive to anhedral fine-grained and dark green with a saccharoidal texture; type II shows well-formed crystals with a green to white colored form from the epidote-clinozoisite series; type III displays disseminated fine-grained pink piemontite and type IV exhibit thin, fine-grained veinlets of epidote. Type II and III are predominant with mineralization. Quartz is most ubiquitous around veins and breccias. It shows four styles, from oldest to youngest, consisting of type I as fine-grained; type II as medium-grained to coarse-grained; type III is fine grained with many small spots and type IV displays thin chalcedony veinlets. The first type forms as patches within red breccia matrix. Type II and III show opaque minerals dominated by chalcocite, chalcopyrite, rare bornite, electrum, and native gold. Type III is associated with specular hematite in ore-bearing samples. Chlorite is a common mineral where alteration has occurred. At least two types of chlorite (I and II) were identified. Type II chlorite are Fe-rich laths with blue interference colour and darker than those of type I. In contrast, chlorite of type I is more widespread at shallower levels in the volcanic strata.

The mineralized parts are either massive and continuous as veins (Fig. 8D), or irregular and discontinuous as thin veinlets, or disseminated (Fig. 8E). The mineralization is relatively simple, with the most abundant primary ore minerals chalcopyrite, chalcocite, and lesser amount of bornite with a smaller abundance of specular hematite, pyrite, and galena. Other uncommon opaque minerals recognized by the EPMA were comprised of gold-bearing minerals as electrum (51.7% to 54.42% Au, 34.6% to 40.32% Ag) or as pyrite and native gold, spread across the quartz crystals (74.21% to 95.41% Au). X-ray diffraction analysis determined secondary minerals such as chalcocite, djurleite, digenite, covellite, and rare native copper. Petrographic examinations of polished blocks and polished thin sections show that copper mineralization normally occurs as open-space filling, breccia filling, disseminations, amygdule-fillings, and in replacement textures.

The age of mineralization is poorly constrained and could range from at least Late Oligocene to Miocene or even younger. Based on mineralization features (textural and mineralogical) and the relative timing of veins, these may be subdivided into pre-ore, ore stage (Fig. 9), and supergene stage. At least, three episodes of mineralization are recognized based on crosscutting relationships in the surface outcrops and drill core logging that are divided into three subzones.

The pre-ore stage alteration is comprised of a fine-grained epidote-quartz-calcite assemblage with minor chlorite, prehnite, pumpellyite, and actinolite, initially affecting a large volume of the host basaltic andesite as replacement and dissemination. Despite the wide distribution of pale-green alteration, this first stage is barren.

4.4.1. Ore stage I

The first event of mineralization starts with the red breccia (Fig. 9A). This breccia is cemented by precipitation of medium-grained quartz and coarse-grained calcite associated with chalcopyrite and pyrite situated along fragment margins. However, most of the sulfides

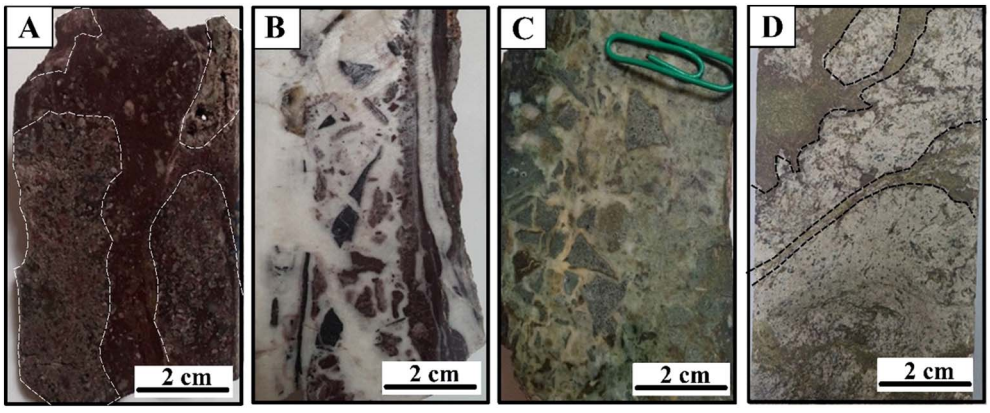

Fig. 7. Photographs of drill cores exhibiting three types of breccia from the Hendou-abad mineral district. (A) Hand sample of red breccia cemented by calcite and fine quartz with large rounded fragments. Oxidized residual chalcopyrite and pyrite are found along fragment margins. Voids are filled with calcite and gypsum. (B) Silica breccia with two types of fragments including red breccia and volcanic rock fragments. Note the long clasts in contact margin of silica breccia. (C) Angular-shaped fragments in hydraulic epidote breccia. (D) Rounded large clasts in contact margin of epidote breccia.

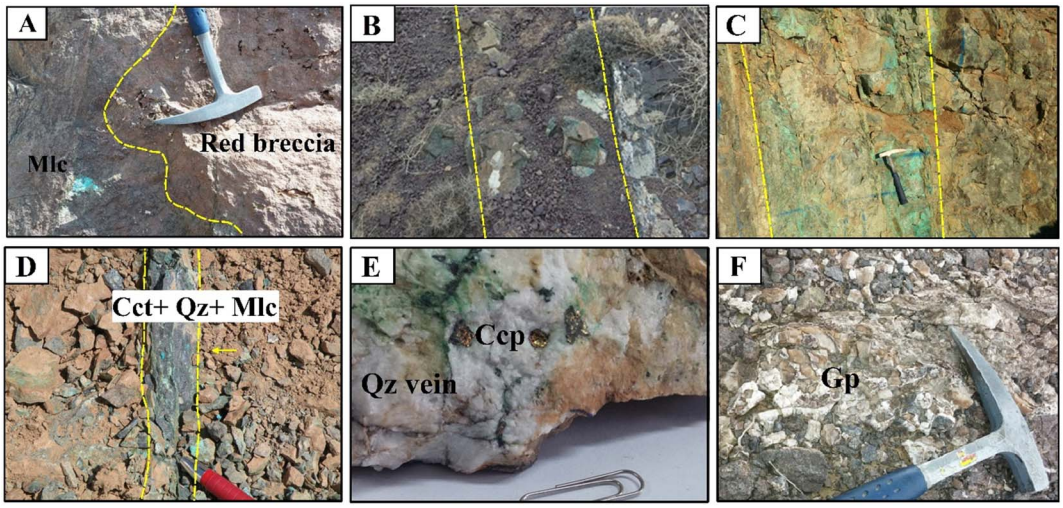

Fig. 8. Geometry of breccia, late dike, and mineralization. (A) Undulating contact of red breccia with the host basaltic andesite. Note fine voids in breccia at top portion of picture. (B) Chalcocite-bearing quartz vein with sharp boundary parallel to the late dike. Altered late dike intruded weathered basaltic andesite. (C) Type IV epidote as veinlets that penetrated the late dike. Malachite masses cutting through epidote veinlets seem to occur in the supergene condition. Note the alteration margin in the host rock around the late dike. (D) Malachite and quartz along with massive chalcocite vein. (E) Chalcopyrite in gold-bearing quartz vein. (F) Large voids in breccia are filled by gypsum.

in the red breccia are replaced by secondary Fe-oxide. In addition to this episode, late dikes intrude the red breccia. Sulfide minerals in red breccia weathered extensively during initial exhumation, uplift, and oxidation.

4.4.2. Ore stage II

This event is dominated by deposition of medium-grained to coarse-grained epidote + quartz + calcite ± titanite along with chalcopyrite and major primary chalcocite with clear cleavage, as well as trace amounts of bornite, pyrite, electrum, galena, and specular hematite (Fig. 9B). Quartz and epidote minerals, with the intensity of alteration increase towards copper ore. Textural relationships indicate that the ore stage II occurs as two distinct styles: a) chalcopyrite, chalcocite, galena, and pyrite as disseminated euhedral crystals (Fig. 9C); and b) as intergrown chalcopyrite-chalcocite-bornite in veinlets (Fig. 9D). Galena is fine-grained to medium-grained (< 50 to 150 μm). White breccia (Fig. 7B) is formed in the beginning of this stage during a short time span.

4.4.3. Ore stage III

The final stage is represented by secondary chalcocite + bornite + chalcopyrite (Fig. 9E) as major high-grade copper phases occurring as veinlet and vacuole filling (Fig. 9F), which is enveloped by a propylitic alteration halo. The associated gangue minerals adjacent to veins are medium-grained to coarse-grained epidote, quartz, and calcite. Green breccia is associated with this stage (Fig. 7C). Chalcocite veinlets form in the cement.

The supergene mineral assemblage is the final stage consisting of high-grade silver-bearing minerals such as digenite, covellite, and djurleite, but also gold-bearing minerals with Fe-oxides. Oxidized ore consists of malachite, azurite, and goethite. The gangue minerals accompanying this stage are fine-grained quartz, late calcite, gypsum

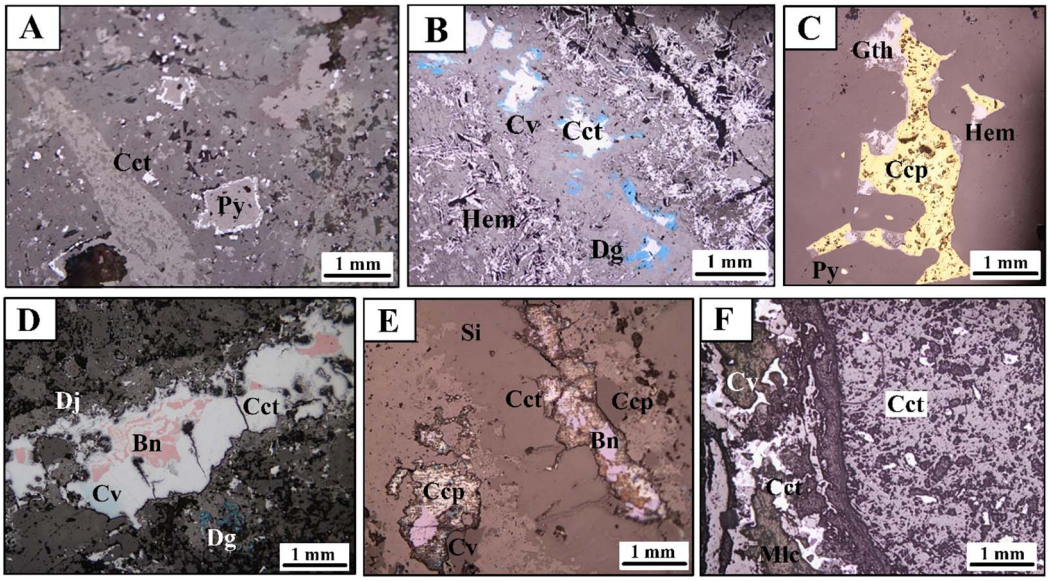

Fig. 9. Photomicrographs in reflected light showing (A) Disseminations of euhedral pyrite in stage I breccia cement that are generally replaced by minor chalcocite from stage III. (B) Specular hematite cut by thin sulfide-quartz vein. Stage II chalcocite replaced by digenite and covelite. (C) Chalcopyrite of stage II in quartz vein, fine rim of tarnish surrounding chalcopyrite. (D) Intergrowth of chalcocite with bornite in stage II. (E) Thin stage II chalcopyrite veinlet replaced by stage III bornite and chalcocite. (F) Fine-grained chalcocite of stage III in wall rock.

(Fig. 8F), and chalcedony occurring as veinlets and open space filling.

5. Geochemical characteristics of Hendou-abad mineral district

5.1. Mineralized rocks

In our set of combined surface bulk-powder samples and drill core samples, copper grades range between 460 and 114,100 ppm, with an average grade of 26,700 ppm. Gold values also indicate a widespread range, from 0.1 to 4.42 ppm. The highest concentration of gold occurs in a chalcopyrite-bearing quartz vein (Fig. 8E). The Ag concentrations of investigated ore samples vary between 1 and 198 ppm, with an average of 61.5 ppm. Additional analyses by EPMA in the copper sulfide minerals show that higher silver grades are found in the secondary copper minerals, especially covellite (Fig. 9B and D). Sulfur contents are generally below 2.11 wt%.

5.2. Dikes

5.2.1. Whole-rock geochemistry of dikes

New major- and trace-element data of two types of dikes are presented in Table 2. Dikes are mainly gabbro and diorite. The rocks used for geochemical data must first be evaluated for their degree of alteration prior to describing primary geochemical properties. The alteration intensity of samples can be recognized using two geochemical indexes: the Ishikawa alteration index (Ishikawa et al., 1976) and the chlorite-carbonate-pyrite index (Large et al., 2001) in the AI [AI = 100 × (MgO + K_2O)/(MgO + K_2O + CaO + Na_2O)] versus CCPI [CCPI = 100 × (FeO + MgO)/(FeO + MgO + Na_2O + K_2O)] plot. The AI versus CCPI plot clearly distinguishes between the least-altered and propylitically altered rock samples. CCPI index values (~75–80) indicate the least altered dike samples. As is shown in Fig. 10A, the intense propylitically altered sample plots outside of the least-altered field towards epidote alteration.

We utilize published data (Table 2) from the Nasrand dikes (Kananian et al., 2014a) analyzed by XRF to explore behavior of trace elements compared to Hendou-abad early dikes. The Nasrand dikes have northwest-southeast orientation similar to the early dikes (for location of Nasrand area, see Fig. 1C).

Least-altered dikes show notable variation in geochemistry with regard to SiO_2 (45.8–52.8 wt%), MgO (5.01–10.14 wt%), alkali content (Na_2O + K_2O 5.4–6.8 wt%), Al_2O_3 (15.7–17.9 wt%), CaO (4.7–8.4 wt %), FeO (7.3–9.5 wt%), P_2O_5 (0.2–0.5 wt%), and TiO_2 content (0.8–1.3 wt%). The dikes are Al-undepleted (Al_2O_3/TiO_2) ratios average 16.8, ranging from 14.8 to 22.3). Most samples are transitional to moderate alkaline in terms of Na_2O + K_2O contents (Table 2). On the other hand, the studied least-altered samples show calc-alkaline affinity in the Y-Zr diagram (Ross and Bedard, 2009; Fig. 10B). Overall, the low SiO_2, and high MgO, Cr, and Ni contents suggest a mantle source rather than a crustal source for the entire set of dike magmas. The recognition of fractionation trends on the Harker diagram is restricted due to the small variation in the content of SiO_2 and MgO within the dikes. Late

Table 2
Major- and trace-element lithogeochemistry from the Hendou-abad mineral district, Iran.

	Nasrand dike					Early dike				Late dike					Host rock	Altered rock
Sample	N33*	A7*	N45*	N38*	N34*	Cu_IS44	Cu_IS101	$Cu_{II}S159$	Cu_IS20	Cu_IS132	BH_5-5.2	BH_{14}-6.5	BH_5-25	$Cu_{II}S161$	$Cu_{II}S75$	$al_{II}S41$
no.						a	a	b	b	a	a	a	a	b	c	d
SiO_2 wwt%	48.18	49.95	53.96	54.93	55.77	45.81	46.72	49.2	52.79	46.73	46.92	48.99	49.87	51	50	59.79
TiO_2	0.94	1.38	0.87	0.95	0.69	1.09	0.90	1.05	0.80	1.06	1.15	1.05	1.01	1.05	1.30	0.70
Al_2O_3	17.49	17.91	18.39	17.99	17.97	16.76	16.97	17.52	17.89	15.71	17.34	16.71	16.91	16.41	16.78	12.42
FeO	11.5	9.7	8.2	9.0	6.99	8.95	9.33	9.38	7.28	7.68	8.9	7.98	7.89	7.36	9.54	8.17
MnO	0.25	0.16	0.16	0.17	0.14	0.38	0.53	0.20	0.14	0.23	0.34	0.20	0.16	0.17	0.17	0.24
MgO	9.31	5.36	5.02	3.72	5.40	6.87	7.68	5.02	5.01	7.81	10.14	6.24	7.06	6.01	5.81	0.30
CaO	8.74	9.43	7.75	6.93	8.38	5.58	5.7	7.1	7.71	8.39	3.92	4.73	4.66	6.51	5.01	15.03
Na_2O	2.17	3.74	3.78	4.11	3.25	4.61	3.97	4.35	3.49	3.5	3.43	3.07	3.31	4.54	5.08	0.21
K_2O	1.08	1.24	0.78	1.07	0.48	1.40	0.92	1.46	0.76	2.09	1.95	2.41	3.51	1.95	1.35	0.06
P_2O_5	0.18	0.45	0.17	0.22	0.14	0.27	0.19	0.28	0.18	0.46	0.41	0.41	0.38	0.39	0.47	0.18
LOI						6.89	5.64	3.43	2.82	5.01	3.95	6.84	3.61	3.05	3.05	1.62
F						0.17	0.15	0.15	0.14	0.15	0.13	0.19	0.12	0.15	0.13	0.13
Cl ppm						114.7	150.2	131.9	85.4	127.9	214.8	149.1	313.3	131.9	130.8	55.2
S						50	75	100	100	150	125	50	50	50	75	50
As						5	28.7	8.1	8.2	5.2	5	24.7	7.8	17.5	5	34.5
Ba	446	357	344	381	234	604.5	466.2	505.2	315.9	603.7	2036.8	1334	4296	784.4	665	9.5
Rb	34.4	24.6	19.9	30.8	24.6	42.3	24.2	58.7	24.6	59.9	74.1	65.1	108.5	49.5	39.3	5
Th	1.5	2.4	1.2	1.5	2.4	3.9	3.1	4.3	3.1	4.9	4.4	3.3	3.2	3.3	–	–
Sr	378	559	387	437	559	202	362	601	380	432	433	319	507	239	366	1414
Zr	60	140	90	100	60	104.5	71.1	91.3	106.2	113.4	119.3	133.4	136.4	132.9	132.0	67.7
Nb	3.4	11.1	3.7	4.5	3.5	7.0	5.1	7.8	5.5	11.1	9.4	14.9	17.0	15.4	6.3	10.0
Ni	103	42.2	37.5	2.5	57.6	42.6	38.1	24.3	33.6	126.4	47.5	61.1	59.2	51.3	14.8	10.6
Pb	5.8	6.0	6.1	7.1	9.0	5.6	40.9	16.0	16.0	9.9	6.2	13.2	3.0	9.4	110.9	120
Co						34.7	34.2	27.4	23.1	32.0	35.2	27.6	28.0	25.1	29.3	4.1
Zn						334.6	681.1	116.8	95.1	286.3	286.4	125.8	140.2	107.2	99.3	15.5
Cr	–	–	70	100	–	60.6	85.9	75.8	43.9	230.3	105.9	128.0	110.6	91.7	38.1	82.7
V	294	264	220	228	192	243.3	249.3	261.1	185.8	197.0	247.0	186.6	200.6	179.9	286.9	322.3
Y	18.8	26.0	19.4	22.0	16.2	22.4	17.8	24.2	25.0	20.2	26.3	22.9	21.6	21.3	28.0	14.8
Ga	18.3	19.0	18.3	19.8	17.8	17.7	20.0	17.1	16.7	16.7	17.5	16.8	12.7	15.6	18.5	27.6
Sc						28.1	26.2	27.1	22.8	18.8	30.3	21.6	19.5	21.4	28.5	21.1
La	10.4	20.5	9.7	13.0	8.9	28.9	21.4	24.4	18.8	35.8	32.1	31.9	41.2	27.0	28.0	25.4
Ce	22.7	44.0	21.2	27.6	19.0	57.7	32.4	48.5	24.8	72.0	44.8	51.3	30.3	54.2	70.9	44.1
Nd	12.9	22.2	11.6	14.8	9.8	16.8	7.3	18.0	12.0	32.7	24.3	30.2	31.6	24.9	26.3	5.2
W						8.2	12.9	8.7	5.2	< 5	7.2	5.9	6.4	11.7	21.7	12.5
Cu						< 10	27	143	43	10	704	< 10	20	310	1450	< 10

Notes: Abbreviations: a gabbro, b pyroxene-bearing diorite, c least-altered trachybasalt, d epidote altered andesite.
* Kananian et al. (2014a).

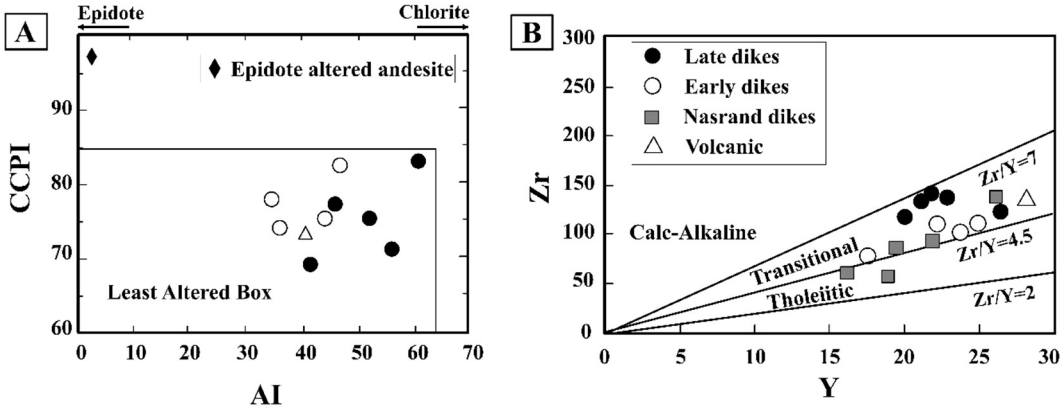

Fig. 10. (A) AI-CCPI alteration diagram. All samples of dikes plot in the least-altered box. (B) Geochemical classification of the Hendou-abad dikes in Zr (ppm) vs. Y (ppm) diagram.

dikes have higher K, P, Zr, Nb, Ti, Cr, Ni, Ba, and Rb compared to early dikes (Table 2). Other major- and trace-element data are similar between late and early dikes.

The Hendou-abad mineral district dike samples display a subduction setting pattern on a MORB-normalized multi-element diagram (Fig. 11A). They are slightly enriched in Rb, K, Sr, and Th, strongly enriched in Ba, and show negative anomalies for Nb and Ti, which are characteristic of arc magmatic systems (Pearce et al., 1984; Tatsumi et al., 1986; Pearce, 2008). Late dikes exhibit slightly higher Ba, Rb, Sr, and K contents than the early dikes (Fig. 11A). The elevated Ba contents may have been introduced by aqueous fluids during subduction processes (Kogiso et al., 1997; Ghatak et al., 2012). Arc maturation is indicated by an increase of Rb/Zr ratios versus Nb content from the early dikes to the late dikes (Fig. 11B). Element ratios such as low Nb/La (0.24–0.57, average of 0.35), low Zr/Y (3.8–6.3, average of 5.02), Ce/Pb (0.79–10.3, average of 5.52), and higher variability seen in Ba/La (16.8–104.3, average of 37.3) may indicate some degree of crustal contamination (e.g., Davidson, 1987; Kerrich et al., 1999; Bohlar et al., 2003). Mafic magmas that undergo crustal contamination commonly show La/Nb ratio > 1.5, and a decrease of Ce/Pb ratios with increasing silica content (Sun et al., 2008). Despite La/Nb (1.8–4.2, average of 3.1), the latter feature is not clearly seen in the dikes from the Hendou-abad mineral district.

On the Th-Zr-Nb ternary diagram (Wood, 1980), the dike samples fall in the calc-alkaline basalt (CAB) field (Fig. 12A), although the late dikes show more enrichment in Nb. The La-Y-Nb ternary diagram (Cabanis and Lecolle, 1989) confirm a continental arc setting for the early dikes, while the late dikes approach the composition of continental basalt (Fig. 12B). On the plot of Ti against Zr designed for distinguishing arc basalt from within-plate and oceanic-floor basalt (Pearce and Gale, 1977), almost all of the dike samples plot in the arc basalt field (Fig. 13A). Although the late dikes show geochemical signatures akin to back-arc intraplate rocks in the Nb versus Zr (Tatsumi et al., 1995; Fig. 13B).

6. Discussion

Geochemical data for dikes, observations of their structural relationship, and investigations of breccia and mineralization are merged to fully consider the spatial relationships between faults, dikes, breccias, and mineralization in the Hendou-abad.

6.1. Dikes emplacement in mineral district

Both the early and late dikes span from gabbro to diorite in composition. They have intruded the Late Eocene-Oligocene volcanic rocks (Fig. 14A) along faults. However, the dikes crosscutting relationships with Oligo-Miocene limestone was observed in the Kasouj area (Fig. 1C), northwest of the study area (Rahimzadeh, 1994). Late dikes also intruded the red breccia (Fig. 14C). Field observations show that the northwest-southeast trending early dikes are steeper dipping and are wider than the east-west trending late dikes. The two groups of dikes show sharp contacts with their country rocks. Chilled margins are consistent with emplacement of both cases in cool host rocks. The lack of any signs of glass in the groundmass in the early dikes demonstrates reheating or a comparably slower cooling rate (Lofgren, 1971). The petrographic examination shows that plagioclase crystallized before pyroxene in the early dikes. Compared with early dikes, the late dikes show greater degrees of alteration intensity. Also, the host rock in contact with altered late dikes has undergone epidote-calcite alteration (Fig. 7C).

The compositional difference between the late dikes and the early

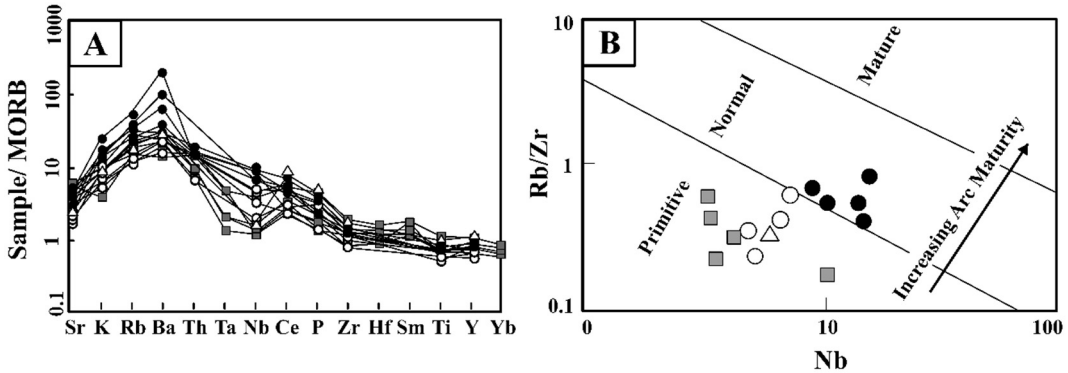

Fig. 11. (A) MORB-normalized plot of Sun and McDonough (1989) illustrates trace elements for early and late dikes of Hendou-abad. (B) Plot of Rb/Zr vs. Nb (ppm) (after Brown et al., 1984). Trend represents maturation of arc from early dikes to late dikes. For symbols see Fig. 10.

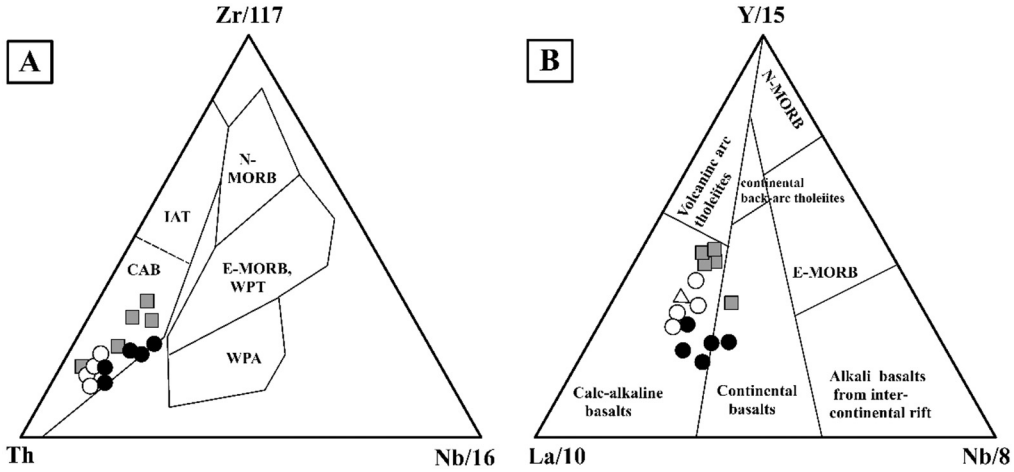

Fig. 12. Tectonic discrimination diagrams for the Hendou-abad dikes, WPA: within plate alkali basalt, CAB: calc-alkaline basalt. Dataset plot in CAB field. For symbols see Fig. 10. (A) Th-Zr/117-Nb/16 subdivision diagram (Wood, 1980). (B) La-Y-Nb discrimination diagram (Cabanis and Lecolle, 1989) for dikes that are the same as in A.

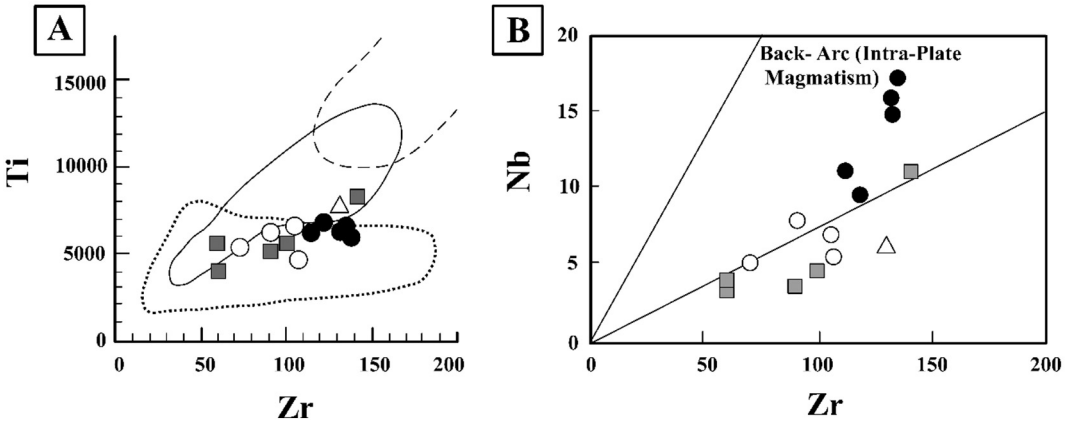

Fig. 13. (A) a plot of the Hendou-abad dikes on the discrimination diagram of Ti (ppm) vs. Zr (ppm) from Pearce and Gale (1977). Dotted line display field of island arc basalts and andesites, the continuous line indicates within-plate of ocean-floor basalts and dashed line present the field of within-plate basalts. (B) a plot of Nb (ppm) vs. Zr (ppm) concentration (Tatsumi et al., 1995). Late dikes display Zr and Nb enrichment compared with the early and Nasrand dikes. For symbols see Fig. 10.

dikes is not particularly great. Early dikes contain slightly lower absolute abundances of incompatible elements. They show a less pronounced negative Sr anomaly, lower Zr, Ti, Nb, and P abundances, a stronger positive Ba anomaly, and higher Rb and K values. Negative Nb, Ti, and P anomalies indicate an arc setting for both generations of dikes. However, considering the magmatic evolution model of Yeganehfar et al. (2013) for the UDMA, it is possible that the higher Nb contents in the late dikes reflect a contribution from an enriched asthenospheric mantle source that gained importance after gradual slab deepening and rollback. The linear distribution of parallel dikes implies an extensional regime. Despite the mostly compressional stress in arcs, extension may occur due to slab detachment or slab roll-back (e.g., Wortel and Spakman, 2000), for example, an extensional regime or at least relaxation of compressional stress after fast Africa-Eurasia convergence rate in response to a collisional event, has been proposed for the Cenozoic porphyry copper deposits along the western Tethyan (Fig. 1A, Bertrand et al., 2014).

In summary, basic magmatism in southeast Ardestan underwent a slight but distinctive change with time. A subduction-modified mantle source produced volumes of basaltic andesite in a primitive arc stage, and this type of arc magmatism is represented by the early dikes. With time, contributions from an enriched asthenospheric mantle source became more and more important, implying that the tectonothermal situation beneath the continental arc had significantly changed. In addition, a change from compression to extension is observed.

6.2. Mineralizing episodes

The Hendou-abad mineralization district is characterized by an intense extent of propylitic alteration (epidote, calcite, and quartz) dominated by copper-rich sulfide minerals. The location of high-grade mineralization is controlled by fractures near the surface, associated with the intersection between east-west and northwest-southeast oriented faults named ZGF and KF, respectively. Although the overall efforts of direct dating of copper mineralization is not present, it indicates that hydrothermal mineralization was introduced within the volcanic sequence at a time coincident with a local extensional regime, which was characterized by the emplacement of mineralized breccias, sheeted quartz and calcite veins, and subordinate late dikes. For this reason, it can be said that breccias and veins occur around and parallel to the late dikes with an east-west trend and that the host rock were altered (< 10 cm thickness) by the late dikes (Fig. 7C). Thus, the mineralized zones show close spatial relationship with the late dikes, breccias, and propylitic zone. The initial widespread alteration and mineralized red breccia may have been generated by the hydrothermal fluids derived from deeper intrusion (s). The parallel orientation and simple pattern observed of the late dikes and veins is consistent with the proposed model of an intrusive body emplacement at deeper levels for copper porphyry systems by Tosdal and Richards (2001). The stage II epidote-calcite alteration resulted from intruded late dikes in Late Eocene volcanic rocks and red breccias (Fig. 14C). The hydrothermal fluids of the *syn*-mineralization green breccia that are associated with the late dikes may have ascended along faults (Fig. 14D). Secondary oxidation of the primary ore deposit occurs after post-emplacement

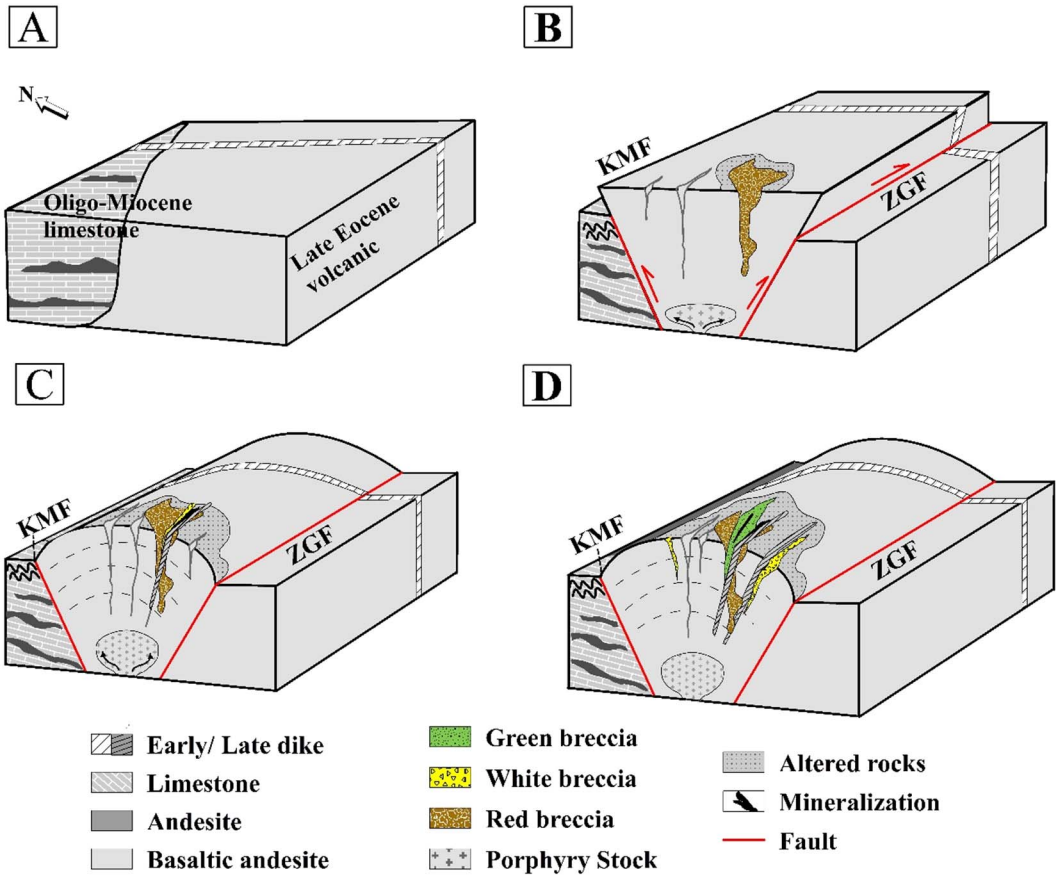

Fig. 14. Schematic model for emplacement of dikes, breccias, and mineralization in Hendou-abad mineral district. (A) the proposed scenario starts at or prior to Miocene, where early dikes intruded Late Eocene volcanic and Oligo-Miocene limestone in north Hendou-abad. (B) rapid uplift in the Hendou-abad is characterized by two principle strike-slip and thrust faults, KMF in the north and ZGF in the south. Initial stages of extensional stress may have occurred because of magma ascending through the upper crust in response to compressional stress resulting from collisional evolution between Africa and Eurasia. Continued uplift is subject to considerable erosion and weathering of red breccia. (C) volatiles seen as mineralized breccias can be released accompanied with the late dikes and probably from the apical intrusive stock at depth. (D) formation of white and green breccias follows during emplacement of the porphyry stock.

processes, as uplift takes place in response to thrust faults and weathering processes start. Overall, the location of the mineralized rocks along faults suggests a genetic connection between these mineralizations and the mineralized breccias and dikes.

6.3. Structural architecture

As described, the copper mineralization events in Hendou-abad are related to two compressive-extensional tectonic cycles. The region was in a collisional evolution between the Arabian and Eurasian plates. Structurally, this compression has generated thrusting, shortening, and vertical thickening of the crust. Faults and dikes in the study area exhibit an unusual trend related to regional strain. The study area is located between KMF and ZGF faults, which are the major branches of the Zefreh Fault, an Eocene-Pliocene fault (Fig. 1C, Berberian, 1976) in the central UDMA. East-west thrust strike-slip faults (KMF and ZGF) and northeast-southwest strike-slip faults formed mainly during the north-south compressional regime (Fig. 1A). Although, the extensional faults may have been generated by the stress of pluton emplacement, and may further have focused the flow of fluids to form vein deposits or breccia pipes. Pre-existing structures in the crust, especially extensional offset zones along trans-lithospheric strike-slip fault systems, possibly will serve to focus magma ascent (Richards, 2005). During the KMF reverse movement (to north side) and ZGF reverse movement (to south side) uplift took place (Fig. 14B). This event has caused increase in volume of mountains and extensional features appearing between both faults, sheeted veins, and folding of Oligo-Miocene limestone in the north part of the KMF (Fig. 14B). However, the orientation of a dike swarm can reflect the vector of extensional stress at the time of their emplacement (Ernst et al., 1995; Gudmundsson and Marinoni, 2002). Dikes are magma-filled channels in which ascent is driven by buoyancy forces induced by hydraulic pressure (Clemens and Mawer, 1992; Richards, 2005). Although, fluid pressures may fluctuate from lithostatic to hydrostatic during porphyry Cu formation (Sillitoe, 2010). We studied the trends of copper veins associated with late dikes to estimate direction of extension stresses at the same time in post Oligocene. Thus, significant features such as linear white breccia and copper and gold vein swarms, combined with parallel dikes would imply a north-south extension in between the faults. Therefore, we suggest that this event might have been accompanied by intrusions of plutons and dikes during maturation of the continental arc. The late dikes are probably situated in the post-collisional uplift stress field (Fig. 14), while the early dikes are intruded during plate collision and active subduction. The weathering, erosion, and corresponding supergene copper enrichment is a response to uplift in our model.

7. Conclusions

The southeast Ardestan copper deposits from the central UDMA occur in altered Late Eocene basaltic andesite rocks. Field observations of this study aimed at understanding the two types of dikes (called early and late), spatially recognized the late dikes associated with mineralized zones. The early dikes were emplaced into Late Eocene-Oligocene rocks (Fig. 14A), including limestone and basaltic andesite

rocks of the Ardestan area. Here, a variety of methods have been used to constrain the genetic link between the dikes, breccias, and mineralization. The geologic evolution of the Hendou-abad copper mineral district is documented and the results applied to interpret two main events of copper deposition, one during the compressional-extensional tectonic force and one during the weathering process.

We propose that the early dikes derived from a subduction-modified mantle in a primitive arc stage during Oligocene or even slightly younger, due to Neotethys ocean closure and its subduction. Generally, crustal extensional stress is developed after compressive stress forces stopped at convergence of plates. This event is supported by the structural pattern and geochemical characteristics of the late dikes. Scilicet, this scenario is the result of the thrust displacements of the KMF fault to the north and the ZGF fault to the south. The southern margin of the Oligo-Miocene limestone formation was affected and folded by the northward movement of the KMF reverse strike-slip fault. During post Oligocene, extensive propylitic halos occur as laterally dominated pipe-like mineralized red breccias, suggesting that an intrusive body may have been emplaced at depth (Fig. 14D). The poor mineralization in red breccia is weathered by rapid uplift and erosion in the southeast Ardestan region. An extensional environment followed and provided fractures for the ascending magmatism and transporting hydrothermal fluid. Late dikes are coeval with an east-west orientation of the stress field and display higher Nb content suggesting genesis in a more mature arc stage than the early dikes. Parallel, thin late dike sets, sheeted hydrothermal veins, and breccias could have resulted from *syn*- and post-mineralization magmatism at depth. It is therefore concluded that the southeast Ardestan copper deposits could represent a porphyry style of features that has been overprinted by later released fluids from folded limestone (north of the study area) as secondary copper mineralization along faults. Although there is no record of porphyry emplacement at the surface, our results for the Hendou-abad mineral district suggest the existence of copper porphyry at depth.

Acknowledgements

We sincerely thank Prof. David R. Lentz for insightful and thoughtful discussions and editing an early version of this manuscript. We also thank Dr. A.R. Nadimi for valuable assistance in field. The authors thank to Dr. Martiya Sadeghi, Dr. Dick Claeson and anonymous referees for their constructive comments in the completion of this paper. This work was funded by the University of Isfahan and IMIDRO to Maryam Salehi and forms part of her MSc thesis. Whole-rock major element analyses using XRF were carried out at the Salzburg University, Austria.

References

Afzal, P., Fadakar Alghalandis, Y., Moarefvand, P., Rashidnejad Omran, N., Asadi Haroni, H., 2012. Application of power-spectrum–volume fractal method for detecting hypogene, supergene enrichment, leached and barren zones in Kahang Cu porphyry deposit, Central Iran. J. Geochem. Explor. 112, 131–138.

Agard, P., Omrani, J., Jolivet, L., Mouthereau, F., 2005. Convergence history across Zagros (Iran): constraints from collisional and earlier deformation. Int. J. Earth Sci. 94 (401), 419.

Agard, P., Omrani, J., Jolivet, L., Whitechurch, H., Vrielynck, B., Spa kman, W., Monie, P., Meyer, B., Wortel, R., 2011. Zagros orogeny: a subduction-dominated process. Geol. Mag. 48 (5–6), 692–725.

Aghazadeh, M., Badrzadeh, Z., 2015. Geology and U-Pb age dating of intrusive bodies in the Sungun deposit. Petrology 22 (6), 1–24 (in Persian).

Alaminia, Z., Karimpour, M.H., Homam, S.M., Finger, F., 2013. The magmatic record in the Arghash region (northeast Iran) and tectonic implications. Int. J. Earth Sci. 102, 1603–1625.

Alavi, M., 1996. Tectonostratigraphic synthesis and structural style of the Alborz Mountain system in northern Iran. J. Geodyn. 21, 1–33.

Alavi, S.G., Hosseinzadeh, M.R., Moayyed, M., 2014. Petrography and petrology of the Sungun porphyry copper deposit and post mineralization dykes with a view to Skarn mineralization (north of Varzeghan, East Azarbaijan). Petrology 17, 17–32.

Arvin, M., Dargahi, S., Babaei, A.A., 2003. Petrogenesis and origin of the Chenar granitoid stock, NW of Kerman, Iran: evidence of Neotethys subduction related arc magmatism. J. Sci. Islam. Repub. Iran 14, 341–350.

Axen, G.J., Lam, P.S., Grove, M., Stockli, D.F., Hassanzadeh, J., 2001. Exhumation of the west central Alborz Mountains, Iran, Caspian subsidence, and collision-related tectonics. Geology 29, 559–562.

Ayati, F., Yavuz, F., Asadi, H.H., Richards, J.P., Jourdan, F., 2012. Petrology and geochemistry of calc-alkaline volcanic and subvolcanic rocks, Dalli porphyry copper–-gold deposit, Markazi Province, Iran. Int. Geol. Rev. 1, 1–27.

Azizi, H., Moinevaziri, H., 2009. Review of the tectonic setting of Cretaceous to Quaternary volcanism in northwestern Iran. J. Geodyn. 47, 167–179.

Bahroudi, A., Fonoudi, M., 2000. Shahrab Geological Map Quadrangle, Scale 1:100000. Geological Survey of Iran, Tehran.

Berberian, M., 1976. Contribution to the seismotectonics of Iran (Part II). Geol. Surv. Iran, Rep. 39 (518p.).

Berberian, F., Berberian, M., 1981. Tectono-plutonic episodes in Iran. In: Gupta, H.K., Delany, F.M. (Eds.), Zagros, Hindu Kush, Himalaya, Geodynamic Evolution. American Geophysical Union Geodynamics Series 3pp. 5–32.

Berberian, M., King, G.C.P., 1981. Towards a paleogeography and tectonic evolution of Iran. Can. J. Earth Sci. 18, 210–265.

Bertrand, G., Guillou-Frottier, L., Loiselet, C., 2014. Distribution of porphyry copper deposits along the western Tethyan and Andean subduction zones: Insights from a paleotectonic approach. Ore Geol. Rev. 60, 174–190.

Beygi, S., Nadimi, A., Safaei, H., 2016. Tectonic history of seismogenic fault structures in Central Iran. J. Geosci. 61, 127–144.

Bohlar, R., Woodhead, J.D., Hertg, J.M., 2003. Continental setting inferred for emplacement of the 2.9-2.7 Ga Belingwe Greenstone belt, Zimbawe. Geology 31 (4), 295–298.

Brown, G.C., Thorpe, R.S., Webb, P.C., 1984. The geochemical characteristics of granitoids in contrasting arcs and comments on magma sources. J. Geol. Soc. Lond. 141, 413–426.

Cabanis, B., Lecolle, M., 1989. Le diagramme La-Y-Nb: un outil pour la discrimination des series volcaniques et la mise en evidence des processus de melange. Compte Rendus de l'Academie des Sciences Series II. 309. pp. 2023–2029.

Chiu, H.Y., Chung, S.L., Zarrinkoub, M.H., Mohammadi, S.S., Khatib, M.M., Iizuka, Y., 2013. Zircon U-Pb age constraints from Iran on the magmatic evolution related to Neotethyan subduction and Zagros orogeny. Lithos 162–163, 70–87.

Clemens, J.D., Mawer, C.K., 1992. Granitic magma transport by fracture propagation. Tectonophysics 204, 339–360.

Dargahi, S., Arvin, M., Pan, Y., Babaei, A., 2010. Petrogenesis of post-collisional A-type granitoids from the Urumieh–Dokhtar magmatic assemblage, Southwestern Kerman, Iran: constraints on the Arabian–Eurasian continental collision. Lithos 115, 190–204.

Davidson, J.P., 1987. Crustal contamination versus subduction zone enrichment: examples from the Lesser Antilles and implications for mantle source compositions of island arc volcanic rocks. Geochim. Cosmochim. Acta 51, 2185–2198.

Ernst, R.E., Head, J.W., Parfitt, E., Grosfils, E., Wilson, L., 1995. Giant radiating dyke swarms on Earth and Venus. Earth-Sci. Rev. 39, 1–58.

Fotoohirad, G.R., Droop, G.T.R., Burgess, R., 2009. Early Cretaceous exhumation of high-pressure metamorphic rocks of the Sistan Suture Zone, eastern Iran. Geochem. J. 44, 104–116.

Ghasemi, H., Rezaei, M., 2015. Petrochemistry and tectonic setting of the Davarzan-Abbasabad Eocene Volcanic (DAEV) rocks, NE Iran. Mineral. Petrol. 109 (2), 235–252.

Ghasemi, A., Talbot, C.J., 2006. A new tectonic scenario for the Sanandaj-Sirjan zone (Iran). J. Asian Earth Sci. 26, 683–693.

Ghatak, A., Basu, A.R., Wakabayashi, J., 2012. Elemental mobility in subduction metamorphism: Insight from metamorphic rocks of the Franciscan complex and the Feather River ultramafic belt, California. Int. Geol. Rev. 54, 654–685.

Ghazi, A.M., Hassanipak, A.A., 1999. Geochemistry of subalkaline and alkaline extrusives from the Kermanshah ophiolite Zagros suture zone, western Iran: implications for Tethyan plate tectonics. J. Asian Earth Sci. 17, 319–332.

Ghorbani, M.R., 2006. Lead enrichment in Neotethyan volcanic rocks from Iran: the implications of a descending slab. Geochem. J. 40, 557–568.

Gudmundsson, A., Marinoni, L.B., 2002. Geometry, emplacement and arrest of dykes. Ann. Tecto. 13, 71–92.

Harzhauser, M., Piller, W.E., 2007. Benchmark data of a changing sea-Palaeogeography, palaeobiogeography and events in the Central Paratethys during the Miocene. Palaeogeogr. Palaeoclimatol. Palaeoecol. 253, 8–31.

Hessami, K., Jamali, F., Tabassi, H., 2003. Major Active Faults of Iran: Tehran. Ministry of Science, Research and Technology, International Institute of Earthquake Engineering and Seismology (scale 1:2500000).

Ishikawa, Y., Sawaguchi, T., Iwaya, S., Horiuchi, M., 1976. Delineation of prospecting targets for Kuroko deposits based on modes of volcanism underlying dacite and alteration halos. Min. Geol. 26, 105–117.

Jabbari, A., Ghorbani, M., Koepke, J., Torabi, G., Shirdashtzadeh, N., 2010. Petrography and mineral chemistry of basaltic dykes in the west of Borooni (SW of Ardestan, Iran): evidences of magma mixing. Petrology 1 (2), 17–30 (in Persian with English abstract).

Jebrak, M., 1997. Hydrothermal breccias in vein-type ore deposits: a review of mechanisms, morphology and size distribution. Ore Geol. Rev. 12, 111–134.

Kananian, A., Hamzei, Z., Sarjoughian, F., Ahmadian, J., 2014a. Origin and tectonic setting of granitic rocks and dolerite dikes in the Nasrand pluton, southeast of Ardestan. Petrology 17, 103–118 (In persian with English abstract).

Kananian, A., Sarjoughian, F., Nadimi, A., Ahmadian, J., Ling, W., 2014b. Geochemical characteristics of the Kuh-e Dom intrusion, Urumieh–Dokhtar magmatic arc (Iran): implications for source regions and magmatic evolution. J. Asian Earth Sci. 90, 137–148.

Kerrich, R., Wyman, D.A., 1997. Review of developments in trace-element fingerprinting of geodynamic settings and their implications for mineral exploration. Aust. J. Earth

Sci. 44, 465–487.
Kerrich, R., Polat, A., Wyman, D., Hollings, P., 1999. Trace element systematic of Mg- to Fe-tholeiitic basalt suites of the superior province: implications for Archean mantle reservoirs and greenstone belt genesis. Lithos 46, 163–187.
Kogiso, T., Tatsumi, Y., Shimoda, G., Barsczus, H.G., 1997. High μ (HIMU) ocean island basalts in southern Polynesia: new evidence for whole mantle scale recycling of subducted oceanic crust. J. Geophys. Res. 102, 148–227.
Large, R.R., Gemmell, J.B., Paulick, H., 2001. The alteration box plot-a simple approach to understanding the relationship between alteration mineralogy and litho-geochemistry associated with volcanic-hosted massive sulfide deposits. Econ. Geol. 96, 957–971.
Laznicka, P., 1988. Breccias and coarse fragmentites. Dev. Econ. Geol. 25, 832.
Lofgren, G., 1971. Spherulitic texture in glassy and crystalline rocks. J. Geophys. Res. 76, 5635–5648.
Mohajjel, M., Fergusson, C.L., Sahandi, M.R., 2003. Cretaceous-Tertiary convergence and continental collision, Sanandaj-Sirjan Zone, western Iran. J. Asian Earth Sci. 21, 397–412.
Mohammadi, S., 2016. Structural Analysis of Southeast Ardestan Area for Determination the Relationship between Mineralization and Structural Elements. MSc Thesis. University of Isfahan, Iran (135 p.).
Moinvaziri, H., 1985. Volcanisme Tertiaire et Quaternaire en Iran. PhD Thesis. Orsay, Paris-Sud (290 p.).
Morley, C.K., Kongwung, B., Julapour, A.A., Abdolghafourian, M., Hajian, M., Waples, D., Warren, J., Otterdoom, H., Srisuriyon, K., Kazemi, H., 2009. Structural development of a major late Cenozoic basin and transpressional belt in central Iran: the Central Basin in the Qom–Saveh area. Geosphere 5, 325–362.
Pearce, J.A., 2008. Geochemical fingerprinting of oceanic basalts with applications to ophiolite classification and the search for Archean oceanic crust. Lithos 100, 14–48.
Pearce, J.A., Gale, G.H., 1977. Identification of ore-deposition environment from trace element geochemistry of association igneous host rocks. In: Norry, M.J. (Ed.), Volcanic Processes in Ore Genesis. 7. Geological Society of London, pp. 14–24.
Pearce, J.A., Lippard, S.J., Roberts, S., 1984. Characteristics and tectonic significance of supra-subduction zone ophiolite. In: Kokelaar, B.P., Howells, M.F. (Eds.), Marginal Basin Geology. 16. Geological Society of London, Special Publication, pp. 77–94.
Radfar, J., Amini Chehragh, M.R., 1999. Ardestan Geological Map Quadrangle, Scale 1:100000. Geological Survey of Iran, Tehran.
Rahimzadeh, F., 1994. Treatise on the Geology of Iran: Oligocene-Miocene, Pliocene Geological Plan of the Book. Number 12, Ministry of Mines and Metals. Geological Survey of Iran, Tehran, Iran 311 p.. (In persian).
Richards, J.P., 2005. Cumulative factors in the generation of giant calc-alkaline porphyry Cu deposits. In: Porter, T.M. (Ed.), Super Porphyry Copper and Gold Deposits: a Global Perspective. 1. PGC Publishing, Adelaide, pp. 7–25.
Richards, J.P., Sholeh, A., 2016. The tethyan tectonic history and Cu-Au metallogeny of Iran. In: Economic Geology, Special Publication. 19. pp. 193–212.
Ross, P.S., Bedard, J.H., 2009. Magmatic affinity of modern and ancient sub-alkaline volcanic rocks determined from trace-element discriminant diagrams. Can. J. Earth Sci. 46, 823–839.
Rosseti, F., Nasrabady, M., Gianluca, V., Thomas, T., Axel, G., Mohammad, H., Hosein, M., 2010. Early Cretaceous migmatitic mafc granulites from the Sabzevar range (NE Iran): implications for the closure of the Mesozoic peri-Tethyan oceans in central Iran. Terra Nova 22, 26–34.
Sadeghian, M., Ghaffary, M., 2011. The petrogenesis of Zafarghand granitoid pluton (SE of Ardestan). Petrology 6, 47–70 (In persian with English abstract).
Sarjoughian, F., 2017. The evaluation of physico-chemical parameters of the Nasrand Plutonic complex by using mineral composition. J. Econ. Geol. 8 (2), 307–323.
Sarjoughian, F., Kananian, A., 2017. Zircon U-Pb geochronology and emplacement history of intrusive rocks in the Ardestan section, central Iran. Geol. Acta 15, 25–36.
Schuster, F., Wielandt, U., 1999. Oligocene and Early Miocene coral faunas from Iran: paleoecology and paleobiogeography. Int. J. Earth Sci. 88, 571–581.
Sengor, A.M.C., 1990. A new model for the late Paleozoic–Mesozoic tectonic evolution of Iran and implications for Oman. In: Robertson, A.H.F., Searle, M.P., Ries, A.C. (Eds.), The Geology and Tectonics of the Oman Region. 49. Geological Society London, Special Publication, pp. 797–831.
Shahabpour, J., 1982. Aspects of Alteration and Mineralization at the SarCheshmeh Copper-Molybdenum Deposit, Kerman, Iran. PhD Thesis. Leeds University (342 p.).
Shahabpour, J., 2005. Tectonic evolution of the orogenic belt in the region located between Kerman and Neyriz. J. Asian Earth Sci. 24 (4), 405–417.
Shahabpour, J., 2007. Island-arc affinity of the Central Iranian Volcanic Belt. J. Asian Earth Sci. 30, 652–665.
Sillitoe, R.H., 2010. Porphyry copper systems. Econ. Geol. 105, 3–41.
Sun, S.S., McDonough, W.F., 1989. Chemical and isotopic systematics of oceanic basalts: implications for mantle composition and processes. In: Saunders, A.D., Norry, M.J. (Eds.), Magmatism in the Ocean Basins. 42. Geological Society of London, Special Publication, pp. 313–345.
Sun, M., Yuan, C., Xiao, W.J., Long, X.P., Xia, X.P., Zhao, G.C., 2008. Zircon U–Pb and Hf isotopic study of gneissic rocks from the Chinese Altai: progressive accretionary history in the early to middle Palaeozoic. Chem. Geol. 247, 352–383.
Tatsumi, Y., Hamilton, D.L., Nesbitt, R.W., 1986. Chemical characteristics of fluid phase released from a subducted lithosphere and origin of arc magmas: evidence from high pressure experiments and natural rocks. J. Volcanol. Geotherm. Res. 29, 293–309.
Tatsumi, Y., Kogiso, T., Nohda, S., 1995. Formation of a third volcanic chain in Kamchatka: generation of unusual subduction-related magmas. Contrib. Mineral. Petrol. 120, 117–128.
Taylor, R., 2009. Ore Textures: Recognition and Interpretation. Springer (288 p.).
Tosdal, R.M., Richards, J.P., 2001. Magmatic and structural controls on the development of porphyry Cu ± Mo ± Au deposits. Soc. Econ. Geol. 14, 157–181.
Verdel, C., Wernicke, B.P., Hassanzadeh, J., Guest, B., 2011. A Paleogene extensional arc flare-up in Iran. Tectonics 30 (TC3008).
Vincent, S.J., Allen, M.B., Ismail-Zadeh, A.D., Flecker, R., Foland, K.A., Simmons, M.D., 2005. Insights from the Talysh of Azerbaijan into the Paleogene evolution of the South Caspian region. Geol. Soc. Am. Bull. 117, 1513–1533.
Walker, R., Jackson, J., 2004. Active tectonics and late Cenozoic strain distribution in central and eastern Iran. Tectonics 23 (TC5010).
Whitney, D., Evans, B., 2010. Abbreviations for names of rock-forming minerals. Am. Mineral. 95, 185–187.
Wood, D.A., 1980. The application of a Th-Hf-Ta diagram to problems of tectomagmatic classification and to establishing the nature of crustal contamination of basaltic lavas of the British Tertiary Volcanic Province. Earth Planet. Sci. Lett. 50 (1), 11–30.
Wortel, M., Spakman, W., 2000. Subduction and slab detachment in the Mediterranean-Carpathian region. Science 290, 1910–1917.
Yeganehfar, H., Ghorbani, M.R., Shinjo, R., Ghaderi, M., 2013. Magmatic and geodynamic evolution of Urumieh–Dokhtar basic volcanism, Central Iran: major, trace element, isotopic, and geochronologic implications. Int. Geol. Rev. 55, 767–786.